Imaging Surface Plasmons: From Leaky Waves to Far-Field Radiation

Aurélien Drezet*
Institut Néel, UPR 2940, CNRS-Université Joseph Fourier, 25, rue des Martyrs, 38000 Grenoble, France

Cyriaque Genet
ISIS, UMR 7006, CNRS-Université de Strasbourg, 8, allée Monge, 67000 Strasbourg, France
(Received 22 February 2013; published 21 May 2013)

We show that, contrary to the common wisdom, surface plasmon poles are not involved in the imaging process in leakage radiation microscopy. Identifying the leakage radiation modes directly from a transverse magnetic potential leads us to reconsider the surface plasmon field and unfold the non-plasmonic contribution to the image formation. While both contributions interfere in the imaging process, our analysis reveals that the reassessed plasmonic field embodies a pole mathematically similar to the usual surface plasmon pole. This removes a long-standing ambiguity associated with plasmonic signals in leakage radiation microscopy.

DOI: 10.1103/PhysRevLett.110.213901 PACS numbers: 42.25.Lc, 42.70.−a, 73.20.Mf

Surface plasmon (SP) optics has become a mature and extended field of research, ranging from the development of new optical nanodevices and nanoantennas to the renewal of integrated quantum optics [1,2]. In this context, surface plasmon imaging techniques are of critical importance to the researcher, among which leakage radiation microscopy (LRM) is now emerging as a powerful tool [3,4]. As a far-field optical method, LRM is used for analyzing SP modes both in direct and Fourier (momentum) spaces and it has been successfully implemented in various plasmonic systems, both at the classical and quantum levels [5–10]. Yet, there is still no satisfying theoretical definition of the SP field in an imaging context. Instead, recent reference work on leaky waves have focused on semi-infinite air-metal interfaces, a configuration not relevant to LRM [11–14]. This has fuelled recent debates concerning the precise relation between experimentally recorded images and SP modes [15–17].

In this Letter, we instead propose a novel approach to the problem of leaky waves that provides a full analytical theory of the coherent SP imaging process in the case of a pointlike radiating electric dipole located in air above a thin metal film. This leads us to a new definition of the SP field as a Fano-type interfering component of the imaged radiation. We derive analytical expressions for the far-field radiation that meets all the necessary conditions prescribed to the leakage field symmetries [18]. Importantly, we show that our approach naturally makes the SP field free from the long standing ambiguities of the historical Zenneck and Sommerfeld solutions [19,20] and removes the field discontinuity at the leakage radiation (LR) angle, which was, until now, problematic. Doing so, we also identify the contribution of a lateral wave thus far unnoticed that we associate with a new type of Goos-Hänchen effect in transmission.

In the geometry considered in Fig. 1, a harmonically radiating pointlike dipole $\boldsymbol{\mu} e^{-i\omega t}$ drives a SP wave that leaks through the film in medium 3 and then propagates in the matching oil of the high numerical aperture (NA) immersion objective required for LRM. Because of the specific dispersion relation of SP waves, LR is emitted at an angle $\vartheta_{\mathrm{LR}} > \vartheta_c = \arcsin[\sqrt{(\varepsilon_1/\varepsilon_3)}]$ defining a radiation

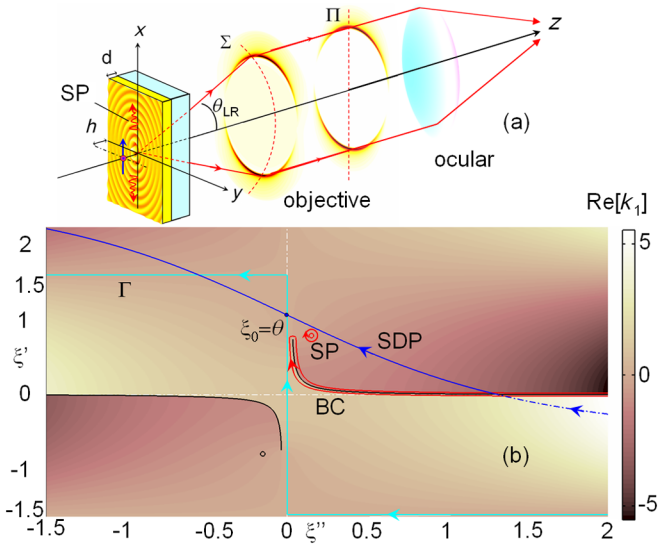

FIG. 1 (color online). (a) Sketch of the leakage radiation microscope: an electric dipole embedded in medium 1 with permittivity $\varepsilon_1 = 1$ (air) is located at $[x = 0, y = 0, z = -h]$ from the surface $z = 0$ of a thin (thickness d) metal film of permittivity ε_2 deposited on a glass substrate of permittivity $\varepsilon_3 = n^2 > \varepsilon_1$ (see [26]). (b) Integration path Γ in the $[\xi'' = \mathrm{Im}(\xi), \xi' = \mathrm{Re}(\xi)]$ complex plane. BC is the branch cut and SP the position of the plasmonic poles (symmetric leaky) in the two $\mathrm{Im}(\xi)\,\mathrm{Re}(\xi) > 0$ quadrants. The steepest-descent path SDP is shown in the $\mathrm{Im}(k_1) > 0$ first R_+ Riemann sheet (continuous line) and in the $\mathrm{Im}(k_1) < 0$ second Riemann sheet (dot-dashed line). The variations of $\mathrm{Re}(k_1)$ are displayed with values given in the color bar.

cone in the forbidden-light sector shown in Fig. 1(a), which intersects the reference sphere Σ of the LRM objective.

Because of the planar symmetry of the problem, the radiated field in medium 3 can be represented in terms of transverse magnetic (TM) and electric (TE) scalar potentials Ψ with $[\boldsymbol{\delta}^2 + k_0^2\varepsilon_3]\Psi_{\mathrm{TM,TE}} = 0$ where $k_0 = \omega/c$. For simplicity, the case of a dipole normal to the film $\boldsymbol{\mu} = \mu_\perp \hat{\mathbf{z}}$ (i.e., $\Psi_{\mathrm{TE}} = 0$) is only discussed here. A general and detailed calculation is given in [21]. Using boundary conditions at the different interfaces, we expand the potential at $[\mathbf{x} = (x, y), z]$ as $\Psi_{\mathrm{TM}}(\mathbf{x}, z) = \int_{-\infty}^{+\infty} k dk A(k, z) H_0^{(+)}(k|\mathbf{x}|)$ with $A(k, z) = (i\mu_\perp/8\pi k_1)\tilde{T}_{13}^{\mathrm{TM}}(k) e^{ik_1 h} e^{ik_3 z}$ and $H_0^{(+)}(k|\mathbf{x}|)$ is the zeroth order radiating-like Hankel function (evolving asymptotically as $e^{+ik|\mathbf{x}|}/\sqrt{k|\mathbf{x}|}$ for large $|\mathbf{x}|$). The Fresnel coefficient $\tilde{T}_{13}^{\mathrm{TM}}(k)$ gives the transmission through the film of TM radiation with a wave vector $|\mathbf{k}| = k$. Stability imposes complex square roots $k_j(k) = \sqrt{k_0^2\varepsilon_j - k^2}$ ($j = 1$ or 3) with $\mathrm{Im}[k_j] \geq 0$.

The precise computation of such a Sommerfeld-like integral is extraordinarily involved due to the presence of two branch cuts associated with $k_{1,3}(k)$ and several SP poles in the complex k plane [22]. To simplify at most the problem, we chose an alternative parametrization of the integral through the complex variable ξ defining $k = k_0 n \sin\xi$. This leaves only one branch cut (BC) $k_1 = k_0\sqrt{\varepsilon_1 - \varepsilon_3 \sin^2\xi}$ with a branch point $\xi = \vartheta_c$. We impose $\mathrm{Im}[k_1] \geq 0$ in the whole complex ξ plane as the choice of the Riemann sheet R_+. The integral becomes

$$\Psi_{\mathrm{TM}}(\mathbf{x}, z) = \int_\Gamma d\xi F(\xi) e^{ik_0 nr\cos(\xi - \vartheta)}, \qquad (1)$$

where $F(\xi) = A(k, d) k k_3 H_0^{(+)}(k|\mathbf{x}|) e^{-ik|\mathbf{x}|}$ with the polar coordinates $|\mathbf{x}| = r\sin\vartheta$, $z = d + r\cos\vartheta$ leading to $(z - d)\cos\xi + |\mathbf{x}|\sin\xi = r\cos(\xi - \vartheta)$. The initial contour Γ corresponding to the condition $\sin\xi$ real is represented on Fig. 1(b).

To evaluate Eq. (1), we deform the contour Γ in order to include the steepest-descent path (SDP) determined by $\mathrm{Im}[f_\vartheta(\xi)] = 1$ with $f_\vartheta(\xi) = i\cos(\xi - \vartheta)$. The SDP crosses Γ at the saddle point $\xi_0 = \vartheta$ defined by $df(\xi)/d\xi = 0$. The SDP contribution Ψ_{SDP} to the field is calculated using the steepest-descent method discussed below. Two additional contributions Ψ_p and Ψ_{BC} associated, respectively, with the SP poles and the BC have to be accounted for when deforming the contour. The most relevant part here is a single SP pole $k_p = k_0 n \sin\xi_p$ resulting from the divergency of $\tilde{T}_{13}^{\mathrm{TM}}(k) = (N_{13}(k)/D_{13}(k))$ when $D_{13}(k_p) = 0$. Such a transcendental equation is known to possess four kinds of SP modes corresponding to leaky waves and bound modes in medium 1 or 3 [4,18]. Importantly on the R_+ sheet, only the leaky mode in medium 3 (labeled symmetric leaky in [18]) is possibly encircled during the contour integration [see Fig. 1(b)] depending on whether $\xi_0 > \vartheta_{\mathrm{LR}}$ or not. This implies that the residue contribution to Ψ_{TM} associated with the SP pole reads

$$\Psi_p = 2\pi i \mathrm{Res}[F(\xi_p)] e^{ik_0 nr\cos(\xi_p - \vartheta)} \Theta(\vartheta - \vartheta_{\mathrm{LR}}), \qquad (2)$$

where $\Theta(x)$ is the Heaviside unit-step function and where the LR angle is precisely defined by $\mathrm{Im}[f_{\vartheta_{\mathrm{LR}}}(\xi_p)] = 1$, i.e., $\vartheta_{\mathrm{LR}} = \mathrm{Re}[\xi_p] + \arccos(1/\cosh\mathrm{Im}[\xi_p]) \simeq \mathrm{Re}[\xi_p]$. An intensity plot of this contribution is displayed on Fig. 2(a) which clearly shows the conical wave front structure emitted at the angle $\arctan(\mathrm{Re}[k_p]/\mathrm{Re}[k_{3p}]) = \mathrm{Re}[\xi_p] \simeq \vartheta_{\mathrm{LR}}$. Remarkably, this conical $\Theta(\vartheta - \vartheta_{\mathrm{LR}})$ wave front removes the power flow divergence in the $z > 0$ direction due to the exponentially growing field associated with Ψ_p in medium 3 [18] and the spatial singularity along the z axis surviving at all distances away from the source induced by the Hankel function [21].

Beyond ϑ_{LR}, $\Psi_p \propto e^{ik_{3p}z} H_0^{(+)}(k_p|\mathbf{x}|)$ [where $k_{3p} := k_3(k_p)$] in direct relation to the original derivation by Zenneck and Sommerfeld of surface waves [19,20]. It corresponds to what modern literature coined as the leaky SP mode [4,18], belonging to the general family of leaky waves discussed for years in the radio antenna community [23]. It is important to realize, however, that this contribution is actually nonphysical, due to the field discontinuity at ϑ_{LR} introduced by the $\Theta(\vartheta - \vartheta_{\mathrm{LR}})$ prefactor. It thus appears necessary to find a genuinely physical definition of a leaky SP wave. We now show that this is only possible by including in our discussion both Ψ_{SDP} and Ψ_{BC} contributions.

The central result of the Letter is that the LRM imaging process is essentially determined by Ψ_{SDP} which is evaluated as [21]

$$\Psi_{\mathrm{SDP}} = e^{ik_0 nr} \sum_{m\in\mathrm{even}} \frac{\Gamma(\frac{m+1}{2})}{m!(k_0 nr)^{(m+1/2)}} \frac{d^m}{d\tau^m} G(0), \qquad (3)$$

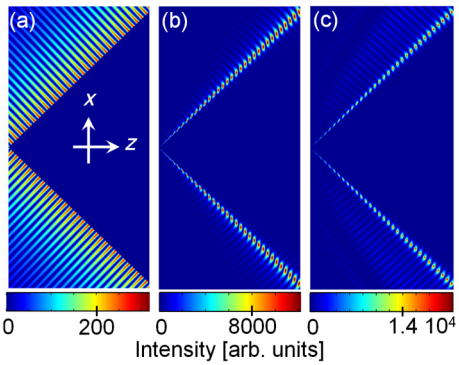

FIG. 2 (color online). Intensity contour plots corresponding to the contributions (a) Ψ_p and (b) Ψ_{SDP}, with their coherent superposition displayed in (c). To remove the asymptotic divergence at infinity we calculated $|\mathbf{x}|(\mathrm{Re}[\mathbf{E}])^2$ in (a), while we calculated instead $r^2(\mathrm{Re}[\mathbf{E}])^2$ in (b),(c).

with the variable $\tau = e^{i\pi/4}\sqrt{2}\sin[(\xi - \vartheta)/2]$ and the function $G(\tau) = F(\xi)(d\xi/d\tau)$ in the vicinity of the saddle point $\tau = 0$ (i.e., $\xi_0 = \vartheta$). A second contribution must be accounted for when $\vartheta > \vartheta_c$ because in this case, the close integration path has to surround the branch cut in the R_+ sheet [see Fig. 1(b)]. Following [24], this contribution can be given as a series expansion

$$\Psi_{\mathrm{BC}} \approx e^{i\Delta\varphi}\Theta(\vartheta - \vartheta_c)\sum_{m=1}^{+\infty}\frac{\alpha_m(r,\vartheta_c)}{[k_0 nr\sin(\vartheta - \vartheta_c)]^{1+m/2}}, \quad (4)$$

where the coefficients $\alpha_m(r, \vartheta_c)$ can be explicitly computed and $\Delta\varphi = k_0 nr\cos(\vartheta - \vartheta_c)$ is interpreted as the phase accumulated by a wave creeping along the metal film (at velocity c) and reemitted at the critical angle ϑ_c (at velocity c/n) [21]. Such a wave is associated in our case to a Goos-Hänchen—like effect in transmission [24]. This contribution is not specific to the LRM geometry but it has never been discussed, whereas the $m = 1$ far-field dominant term in Eq. (4) evolves as $\sim 1/r^2$, i.e., as a Norton wave defined on the same $1/r^2$ order from Ψ_{SDP} [25].

These terms, however, can be neglected in the far field ($r \gg 2\pi/k_0$) where all that survives is the dominant $1/r$ term in the power expansion of $\Psi_{\mathrm{SDP},m=0}$ in Eq. (3). The radiated far field is thus

$$\Psi_{\mathrm{SDP},m=0}(\mathbf{x}, z) \simeq \frac{2\pi k_0 n\cos\vartheta}{ir} e^{ik_0 nr}\tilde{\Psi}_{\mathrm{TM}}[\mathbf{k}, d], \quad (5)$$

where $\tilde{\Psi}_{\mathrm{TM}}[\mathbf{k}, d] = A(k, d)/\pi$ is the bidimensional Fourier transform of $\Psi_{\mathrm{TM}}(\mathbf{x}, z)$ calculated at $z = d$ for the in-plane wave vector $\mathbf{k} = k_0 n\sin\vartheta\mathbf{x}/|\mathbf{x}|$. This expression shows in Fig. 2(b) a conical structure peaked on ϑ_{LR} which should be compared with the one obtained from Ψ_p alone in Fig. 2(a). The comparison with Fig. 2(c) combining both contributions coherently clearly expresses a central result for LRM: $\Psi_{\mathrm{SDP},m=0}$ strongly dominates not only over Ψ_{BC}, as discussed above, but also over Ψ_p, consistently with the finite value of the SP propagation length $L_p = (2\,\mathrm{Im}[k_p])^{-1}$ that overdamps the exponential tail of Ψ_p for angles $\vartheta \geq \vartheta_{\mathrm{LR}}$.

From an imaging perspective, the radiating field given by Eq. (5) is detected in the objective back-focal plane Π sketched in Fig. 1 (see [26]). We plot $I_{\mathrm{TM},\Pi}[\mathbf{k}]$ in Fig. 3 for a dipole either perpendicular or parallel to the interface [28]. We point out that these intensity maps are in quantitative agreement with experiments [4,8,10] and clearly reveal a bidimensional ring with radius $k_r \approx \mathrm{Re}[k_p]$ and width $\delta k \approx 2\,\mathrm{Im}[k_p]$.

As a fundamental paradox, this ring is nowadays associated with the detection of the SP mode [4,29,30] despite the fact that it is Ψ_{SDP} and certainly not Ψ_p which is involved in the measurement process. This paradox stems

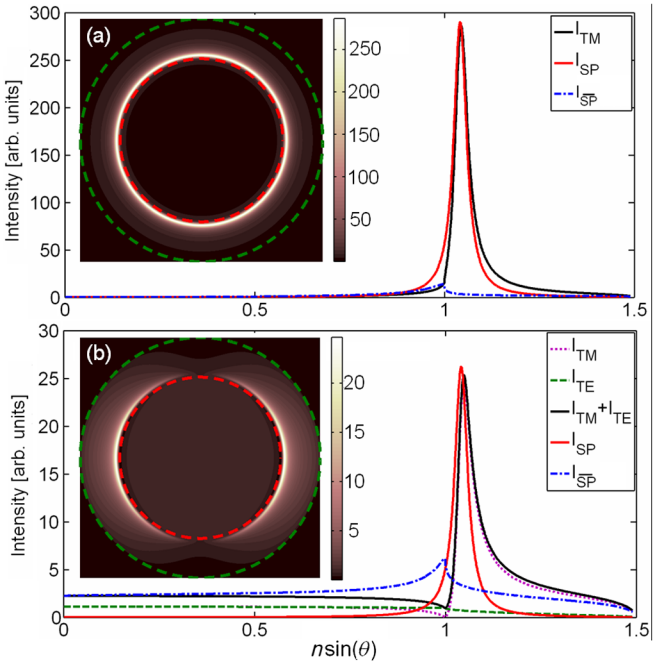

FIG. 3 (color online). Fourier space images recorded in the back-focal plane of the microscope objective for a dipole radiating through a thin metal film, when the dipole is perpendicular (a) or parallel (b) to the metal film. In both cases, the calculated accessible intensities in the $\mathbf{k} = [k_x, k_y]$ plane $I_{\mathrm{TM,TE}}$ are associated with $\tilde{\Psi}_{\mathrm{TM,TE}}$ and I_{SP} with the SP contribution $\tilde{\Psi}_{\mathrm{SP}}$. The nonplasmonic term $I_{\overline{\mathrm{SP}}}$ is defined as a residual $\propto k_0^3 k_3 k^2\varepsilon_3|\tilde{\Psi}_{\mathrm{TM}} - \tilde{\Psi}_{\mathrm{SP}}|^2$ (a) and $\propto k_0^3 k_3 k^2\varepsilon_3|\tilde{\Psi}_{\mathrm{TM}} - \tilde{\Psi}_{\mathrm{SP}}|^2 + I_{\mathrm{TE}}$ (b).

from $G(\tau)$ being singular (thus Ψ_{SDP} too) at the SP pole τ_p (i.e., ξ_p), with a polar contribution $\Psi_{\mathrm{SDP}}^{\mathrm{pole}}$ sharing a closed mathematical relation with Ψ_p. This generated an historical confusion regarding the actual role of SP modes in the Sommerfeld integral, an issue debated since the work of Zenneck and Sommerfeld [11,19,20].

In order to remove the ambiguity, we reconsider the very definition of what the SP field is, by going back to Eq. (3) and observing that $\tilde{\Psi}_{\mathrm{TM}}[\mathbf{k}, d]$ is an explicit function of $k = k_0 n\sin\vartheta$ with $\vartheta \in [0, \pi/2]$. This function can be easily continued over the complex k plane analytically. This function presents some isolated poles such as k_p and $-k_p$ which allow us to decompose $\tilde{\Psi}_{\mathrm{TM}}[\mathbf{k}, d]$ into a regular and polar part. It is this polar part

$$\tilde{\Psi}_{\mathrm{TM}}^{\mathrm{pole}}[\mathbf{k}, d] = \eta_p\frac{1}{\sqrt{k}}\left[\frac{1}{k - k_p} + \frac{1}{i(k + k_p)}\right], \quad (6)$$

with $\eta_p = (i\mu_\perp/8\pi)(k_p/k_{1p})((e^{ik_{1p}h}e^{ik_{3p}d})/(\pi\sqrt{k_p}))\times((N_{13}(k_p))/(\partial D_{13}(k_p)/\partial k_p))$ that we will define as the SP field $\tilde{\Psi}_{\mathrm{SP}}[\mathbf{k}, d] := \tilde{\Psi}_{\mathrm{TM}}^{\mathrm{pole}}[\mathbf{k}, d]$ (see [21] for the general case). To justify this definition, we point out that from Eq. (6) we deduce a SP field $\Psi_{\mathrm{SP}}(\mathbf{x}, z) = \int d^2\mathbf{k}\,\tilde{\Psi}_{\mathrm{TM}}^{\mathrm{pole}}[\mathbf{k}, d]e^{i\mathbf{k}\cdot\mathbf{x}}e^{ik_3(z-d)}$ which, in analogy with

Eq. (1), is alternatively defined by a contour integral over ξ along Γ,

$$\Psi_{\mathrm{SP}}(\mathbf{x}, z) = \int_{\Gamma} d\xi F_{\mathrm{SP}}(\xi) e^{ik_0 nr\cos(\xi-\vartheta)}, \tag{7}$$

where $F_{\mathrm{SP}}(\xi) = \tilde{\Psi}^{\mathrm{pole}}_{\mathrm{TM}}[\mathbf{k}, d] k k_3 H_0^{(+)}(k|\mathbf{x}|) e^{-ik|\mathbf{x}|}$. The remarkable fact about Eq. (7) is that it can be evaluated by the procedures used for Eq. (1) without any branch cut, and split into one contribution from the residue and another from the SDP:

$$\Psi_{\mathrm{SP}}(\mathbf{x}, z) = 2\pi i \mathrm{Res}[F_{\mathrm{SP}}(\xi_p)] e^{ik_0 nr\cos(\xi_p-\vartheta)} \Theta(\vartheta - \vartheta_{\mathrm{LR}}) + e^{ik_0 nr} \sum_{m\in\mathrm{even}} \frac{\Gamma(\frac{m+1}{2})}{m!(k_0 nr)^{(m+1/2)}} \frac{d^m}{d\tau^m} G_{\mathrm{SP}}(0), \tag{8}$$

with $G_{\mathrm{SP}}(\tau) = F_{\mathrm{SP}}(\xi)(d\xi/d\tau)$. Importantly, the residue term in Eq. (8) is identical to Ψ_p given that $\mathrm{Res}[F_{\mathrm{SP}}(\xi_p)] = \mathrm{Res}[F(\xi_p)]$.

In the far field, the $m = 0$ term in the sum dominates and we have $\Psi_{\mathrm{SP}}(\mathbf{x}, z) \simeq (2\pi k_0 n \cos\vartheta/ir) e^{ik_0 nr} \tilde{\Psi}_{\mathrm{SP}}[\mathbf{k}, d]$. In Fig. 3 we compare this expression for Ψ_{SP} to Eq. (5) by computing the intensity in the back-focal plane. In the case of a vertical dipole—Fig. 3(a)—the SP term $I_{\mathrm{SP},\Pi}[\mathbf{k}]$, proportional to $|\tilde{\Psi}_{\mathrm{SP}}[\mathbf{k}, d]|^2$, is quasi-identical to $I_{\mathrm{TM},\Pi}[\mathbf{k}]$. We define the nonplasmonic signal by $I_{\overline{\mathrm{SP}}} \propto |\tilde{\Psi}_{\mathrm{TM}}[\mathbf{k}, d] - \tilde{\Psi}_{\mathrm{SP}}[\mathbf{k}, d]|^2$. In the case of a horizontal dipole—Fig. 3(b)—there is also an additional TE contribution $I_{\mathrm{TE},\Pi}[\mathbf{k}] \propto |\tilde{\Psi}_{\mathrm{TE}}[\mathbf{k}, d]|^2$ to $I_{\overline{\mathrm{SP}}}$. The intensity dip observed for such a horizontal dipole is attributed to a Fano-type interference effect in the $\mathbf{k}$ space between the peaked SP contribution and the broad nonplasmonic signal made explicit by our analysis [31,32].

In a last step, we calculate direct space images through a microscope ocular [see Fig. 1(a)] associated with SP propagation on the metal film by an inverse Fourier transform of the field signal in the Π plane, taking into account the finite angular aperture of the objective [21]. We compare in Figs. 4(a) and 4(b) the images calculated from Eqs. (5) and (8), respectively, for a vertical and a horizontal dipole. Signal differences are more important for a horizontal dipole where TE and TM fields interfere, and decrease for distances larger than $2\pi/k_0$. We point out that the pure SP field at a point $\mathbf{x}'$ of the image plane is given by a simple expression

$$\mathbf{E}_{\mathrm{SP}}(\mathbf{x}') \propto \int_{|\mathbf{k}|\le k_0\mathrm{NA}} d^2\mathbf{k}\sqrt{k_3}\mathbf{k}\tilde{\Psi}_{\mathrm{SP}}[\mathbf{k}, d] e^{i(\mathbf{k}\cdot\mathbf{x}'/M)} = -\int d^2\mathbf{x}\mathbf{D}_{\mathrm{SP},\|}(\mathbf{x}, d)\chi\left(\mathbf{x} + \frac{\mathbf{x}'}{M}\right)\Big/\sqrt{k_{3p}}, \tag{9}$$

where $\mathbf{D}_{\mathrm{SP},\|}(\mathbf{x}, d) = (\partial^2/\partial\mathbf{x}\partial z)\Psi_{\mathrm{SP}}(\mathbf{x}, d)$ is the in-plane component of the SP displacement field along the interface $z = d$ and $\chi(\mathbf{u}) \approx (k_0\mathrm{NA}/2\pi|\mathbf{u}|)J_1(k_0\mathrm{NA}|\mathbf{u}|)$ is the (scalar) point-spread function of the microscope objective.

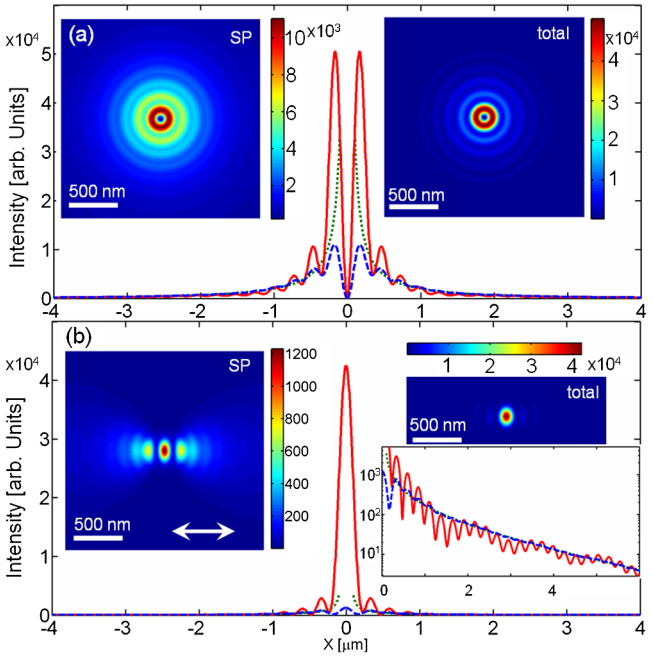

FIG. 4 (color online). Direct space images associated with a pointlike dipole radiating through the metal film and recorded in the back-focal plane of the microscope ocular. (a) Vertical dipole, (b) horizontal dipole (including in this case the additional TE contribution). The red curves correspond to the total signal computed from Eqs. (5) and (9) and the blue ones to the mere SP signal, i.e., Eqs. (8) and (9).

Taking a large microscope magnification $M = nf'/f \ll 1$ (with f, f' being, respectively, the objective and ocular focal lengths) enables us to analyze the recorded images simply using the paraxial-like Eq. (9), despite that leaky waves are emitted in a nonparaxial regime at ϑ_{LR}. Additionally, since $\tilde{\Psi}_{\mathrm{SP}}[\mathbf{k}, d]|$ defines a sharp ringlike distribution, we can approximately write $\mathbf{E}_{\mathrm{SP}}(\mathbf{x}') \propto \mathbf{D}_{\mathrm{SP},\|}(-\mathbf{x}'/M, d)$ for large $|\mathbf{x}'|/M$. Therefore, as shown in Fig. 4, the difference between the real image and the SP field vanishes asymptotically when $|\mathbf{x}'|$ increases. Finally, this analysis shows that only in-plane components of the SP field participate to the image, therefore resolving definitively the current controversy [15–17].

To conclude, we have removed the long-standing ambiguity associated with the very definition of a SP mode as probed in LRM through a revision of the SP field. We have shown how this field interferes, in a Fano-type way, with a broad nonplasmonic radiative signal in the LR imaging process. We expect our findings to have an important impact in the ever-growing field of plasmonics in its different variants: classical to quantum through molecular to nonlinear plasmonics.

This work was supported by Agence Nationale de la Recherche (ANR), France, through the PLASTIPS project and by the French program Investissement d'Avenir (Equipex Union).

*aurelien.drezet@grenoble.cnrs.fr

[1] W. L. Barnes, A. Dereux, and T. W. Ebbesen, Nature (London) **424**, 824 (2003).

[2] M. Agio, Nanoscale **4**, 692 (2012).

[3] B. Hecht, H. Bielefeldt, L. Novotny, Y. Inouye, and D. W. Pohl, Phys. Rev. Lett. **77**, 1889 (1996).

[4] A. Drezet, A. Hohenau, D. Koller, A. Stepanov, H. Ditlbacher, B. Steinberger, F. R. Aussenegg, A. Leitner, and J. R. Krenn, Mater. Sci. Eng. B **149**, 220 (2008).

[5] A. L. Baudrion, F. de Leon-Perez, O. Mahboub, A. Hohenau, H. Ditlbacher, F. J. García-Vidal, J. Dintinger, T. W. Ebbesen, L. Martín-Moreno, and J. R. Krenn, Opt. Express **16**, 3420 (2008).

[6] Y. Gorodetski, K. Y. Bliokh, B. Stein, C. Genet, N. Shitrit, V. Kleiner, E. Hasman, and T. W. Ebbesen, Phys. Rev. Lett. **109**, 013901 (2012).

[7] L. Li, T. Li, S. M. Wang, and S. N. Zhu, Phys. Rev. Lett. **110**, 046807 (2013).

[8] P. Bharadwaj, A. Bouhelier, and L. Novotny, Phys. Rev. Lett. **106**, 226802 (2011).

[9] A. Cuche, O. Mollet, A. Drezet, and S. Huant, Nano Lett. **10**, 4566 (2010).

[10] O. Mollet, S. Huant, G. Dantelle, T. Gacoin, and A. Drezet, Phys. Rev. B **86**, 045401 (2012).

[11] R. E. Collin, IEEE Antennas and Propagation Magazine **46**, 64 (2004).

[12] A. Yu Nikitin, S. G. Rodrigo, F. J. García-Vidal, and L. Martín-Moreno, New J. Phys. **11**, 123020 (2009).

[13] P. Lalanne, J. P. Hugonin, H. T. Liu, and B. Wang, Surf. Sci. Rep. **64**, 453 (2009).

[14] A. Yu Nikitin, F. J. García-Vidal, and L. Martín-Moreno, Phys. Rev. Lett. **105**, 073902 (2010).

[15] J. Wang, C. Zhao, and J. Zhang, Opt. Lett. **35**, 1944 (2010).

[16] L. G. de Peralta, Opt. Lett. **36**, 2516 (2011).

[17] A. Hohenau, J. R. Krenn, A. Drezet, O. Mollet, S. Huant, C. Genet, B. Stein, and T. W. Ebbesen, Opt. Express **19**, 25749 (2011).

[18] J. J. Burke, G. I. Stegeman, and T. Tamir, Phys. Rev. B **33**, 5186 (1986).

[19] J. Zenneck, Ann. Phys. (Berlin) **328**, 846 (1907).

[20] A. N. Sommerfeld, Ann. Phys. (Berlin) **333**, 665 (1909).

[21] See Supplemental Material at http://link.aps.org/supplemental/10.1103/PhysRevLett.110.213901 for mathematical details.

[22] The additional branch cut implied, in principle, by the $1/\sqrt{k|\mathbf{x}|}$ term of the Hankel function can be chosen to be running just below the Γ path with therefore no influence on further contour evaluations.

[23] D. R. Jackson and A. A. Oliner, *Modern Antenna Handbook*, edited by C. A. Balanis (Wiley, New York, 2008), Chap. 7.

[24] L. M. Brekhovskikh, *Waves in Layered Media* (Academic Press, New York, 1960), Chap. 4.

[25] K. A. Norton, Proc. IRE **24**, 1367 (1936).

[26] We model the high NA aplanatic immersion LRM objective by a reference sphere Σ centered on $[x = 0, y = 0, z = 0]$ and of a radius equal to the objective focal length f. The spherical wave front is transformed into a planar wave front Π at the back-focal plane of the objective and converges, after an ocular of focal f', in the image plane Π'. Note that since, $\tan\vartheta_{\mathrm{LR}} \geq 1$, nonparaxial abberations occurring during the propagation from Σ to Π have to be accounted for [27].

[27] W. T. Tang, E. Chung, Y.-H. Kim, P. T. C. So, and C. J. R. Sheppard, Opt. Express **15**, 4634 (2007).

[28] As shown in Fig. 3, vertical dipoles radiate typically 10 times more light than in plane dipoles, meaning (in agreement with experiments [9,27]) that the signal will be, in general, strongly dominated by vertical dipoles (see, however, [3,17]).

[29] L. Novotny, B. Hecht, and D. Pohl, J. Appl. Phys. **81**, 1798 (1997).

[30] R. Marty, C. Girard, A. Arbouet, and G. Colas des Francs, Chem. Phys. Lett. **532**, 100 (2012).

[31] M. Sarrazin, J. P. Vigneron, and J.-M. Vigoureux, Phys. Rev. B **67**, 085415 (2003).

[32] C. Genet, M. P. van Exter, and J. P. Woerdman, Opt. Commun. **225**, 331 (2003).